Journal of Sound and Vibration 330 (2011) 4713–4724

Contents lists available at ScienceDirect

Journal of Sound and Vibration

journal homepage: www.elsevier.com/locate/jsvi

Determination of energy density in ducts by a three-microphone phaseless method and estimation of measurement uncertainties

Jean-Claude Pascal [a,*], Jing-Fang Li [b], Jean-Hugh Thomas [a]

[a] Laboratoire d'Acoustique de l'Université du Maine (CNRS UMR 6613) and Ecole Nationale Supérieure d'Ingénieurs du Mans (ENSIM), Université du Maine rue Aristote, 72000 Le Mans, France

[b] Visual VibroAcoustics, 51 rue d'Alger, 72000 Le Mans, France

ARTICLE INFO

Article history:
Received 4 December 2009
Received in revised form
6 April 2011
Accepted 6 May 2011
Handling Editor: R.E. Musafir
Available online 31 May 2011

ABSTRACT

A new method to measure the total energy density of waves traveling in opposite directions in ducts is suggested in order to completely eliminate phase errors that lead to bias errors and are difficult to control in industrial tests. Only the auto-power spectral densities are measured by the three microphones. The inversion of a linear system based on a propagation model, where the two opposite waves are partially coherent, makes it possible to obtain the energy density. The sensitivity of this method to errors in the speed of sound, errors of microphone calibration and errors of microphone positions in the duct is analyzed. To complete the study on the robustness of the method, an evaluation of the statistical errors is carried out. The total uncertainty is used to make recommendations on the choice of the experimental parameters. The selection of the frequency limits permits to maintain the measurement uncertainty within a given confidence interval.

1. Introduction

The measurement of the total energy density in industrial ducts is often convenient, because the measured value is independent of the position in the acoustic field having incident and reflected components that produce not only interferences (quasi-stationary wave) but also reduction of coherence between the two waves traveling in opposite directions. In a one-dimensional sound field, it is possible to measure the total energy density by the two-microphone method using the finite-difference approximations [1,2]. Although the statistical errors remain limited [3], as well as for the case where the two opposite waves are uncorrelated [4], the measurement is particularly sensitive to phase errors between sensors [2,5], as in the technique to measure the sound intensity [6]. Inverse methods have been employed to obtain the amplitude of waves constituting of the quasi-stationary fields [7], but they are also quite sensitive to the phase errors, unless the number of microphones is largely increased to benefit from the advantage of the over-determined systems. Working with sensors and measurement channels matched in phase is still an important constraint in industrial environments because control and calibration should frequently be carried out to ensure good accuracy. In fact, the sensitivity to the phase errors is much higher than that to the amplitude calibration error, and does not allow the correction of this bias without a significant residual error. Moreover, another method was developed to determine

* Corresponding author. Tel.: +33 2 43 83 39 53; fax: +33 2 43 83 37 94.
E-mail addresses: Jean-Claude.Pascal@univ-lemans.fr (J.-C. Pascal), Jingfang.Li@VisualVibroAcoustics.com (J.-F. Li), Jean-Hugh.Thomas@univ-lemans.fr (J.-H. Thomas).

0022-460X/$ - see front matter © 2011 Elsevier Ltd. All rights reserved.
doi:10.1016/j.jsv.2011.05.006

the quadratic particle velocity from measurements of quadratic pressure and active and reactive sound intensities [5], but it requires the assumption of a perfectly coherent noise field.

A three-microphone method is developed in this paper to determine the total energy density in a duct. Based on an inverse method it uses the measurements of the auto-spectral density of pressure by three microphones and the inversion of a model of partially coherent quasi-stationary waves. This method is well suited for industrial applications, such as the duct elements between an engine and the analyzed system, because it makes the measurement insensitive to the microphone positions. Section 2 describes the principle of measurements. Then in Section 3, the sensitivity of the method to different causes of errors is analyzed. In Section 4 a method is suggested to select the experimental parameters in order to maintain *a priori* the uncertainty of the estimate of the energy density below a pre-defined threshold. The discussion is given in Section 5, which is followed by the conclusion.

2. Principle of the measurements

A general model of one-dimensional partially coherent field can be described by two plane waves traveling in opposite directions

$$p(x,\omega) = A(\omega)e^{-jkx} + B(\omega)e^{jkx}, \tag{1}$$

for which the coherence $\gamma^2_{AB}(\omega)$ between the two wave components can vary from 0 (two independent progressive plane waves) to 1 (stationary wave). $k=\omega/c$ is the wavenumber, with ω the angular frequency and c the speed of sound. The assumption of a plane wave model restricts the validity of the method in the frequency range where all non-planar modes are evanescent (i.e., their amplitudes decay exponentially with distance from the source), resulting in the high frequency limits $f_c \approx 0.59c/D$ and $f_c = 0.5c/L$, respectively, for a circular section of diameter D and a rectangular cross-section $L \times H$ when $L > H$. The potential $V(\omega)$ and kinetic $T(\omega)$ energy densities are expressed in the frequency domain from the power spectral densities (PSD) of the pressure $G_{pp}(\omega)$ and particle velocity $G_{uu}(\omega)$, respectively [1–4]. They can thus be expressed as a function of the auto- and cross-power spectral densities of the amplitudes of the two waves denoted by $G_{AA}(\omega)$, $G_{BB}(\omega)$ and $G_{AB}(\omega)$

$$V(\omega) = \frac{G_{pp}(\omega)}{2\rho_0 c^2} = \frac{G_{AA}(\omega)+G_{BB}(\omega)+2\mathrm{Re}\{G_{AB}(\omega)e^{j2kx}\}}{2\rho_0 c^2}, \tag{2}$$

$$T(\omega) = \frac{\rho_0}{2} G_{uu}(\omega) = \frac{G_{AA}(\omega)+G_{BB}(\omega)-2\mathrm{Re}\{G_{AB}(\omega)e^{j2kx}\}}{2\rho_0 c^2}, \tag{3}$$

where $G_{AB}(\omega) = \gamma_{AB}(\omega)\sqrt{G_{AA}(\omega)G_{BB}(\omega)}e^{j\varphi(\omega)}$ and ρ_0 is the mass density of the fluid. The total energy density is thus written as

$$E(\omega) = V(\omega) + T(\omega) = \frac{G_{AA}(\omega)+G_{BB}(\omega)}{\rho_0 c^2}. \tag{4}$$

Eq. (4) shows that the total energy density is independent of the axial location x. The spectral density $E(\omega)$, obtained from the PSD of pressure and particle velocity (see Eqs. (2) and (3)), is expressed in Joules per cubic meter per Hertz (J/m^3/Hz) and its integration over a frequency band will lead to values in J/m^3. These definitions of the energy densities correspond to a non-dissipative fluid at rest. The proposed three-microphone method gives a local estimate of the energy density at the middle microphone (microphone 2 in Fig. 1). In the case of a weakly dissipative fluid as one encountered in engineering applications, it is usual to consider a non-dissipative fluid model because an error, which is not taken into account in the analysis, will remain low for small microphone spacing. For each microphone positioned at a point x_i on the x-axis ($i=\{1,2,3\}$), the power spectral density (PSD) of the pressure can be written as

$$G_{ii}(\omega) = G_{AA}(\omega) + G_{BB}(\omega) + 2|G_{AB}(\omega)|\cos(2kx_i + \varphi(\omega)), \tag{5a}$$

by considering Eq. (4), Eq. (5a) can be expressed as

$$G_{ii}(\omega) = \rho_0 c^2 E(\omega) + 2|G_{AB}(\omega)|\cos\varphi(\omega)\cos 2kx_i - 2|G_{AB}(\omega)|\sin\varphi(\omega)\sin 2kx_i = a(\omega) + b(\omega)\cos 2kx_i - c(\omega)\sin 2kx_i. \tag{5b}$$

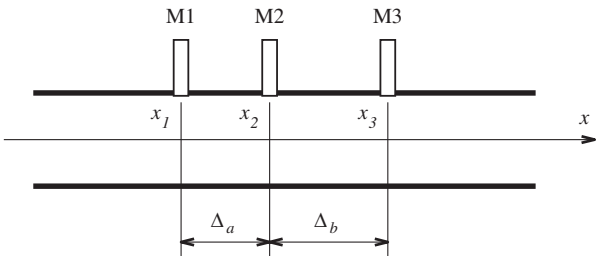

Fig. 1. Positions of three microphones mounted on the duct.

Using at least 3-microphone positions at x_1, x_2 and x_3 (see Fig. 1), the PSD measured can be written in the form of a linear system

$$\begin{bmatrix} G_{11}(\omega) \\ G_{22}(\omega) \\ G_{33}(\omega) \end{bmatrix} = \begin{bmatrix} 1 & \cos 2kx_1 & -\sin 2kx_1 \\ 1 & \cos 2kx_2 & -\sin 2kx_2 \\ 1 & \cos 2kx_3 & -\sin 2kx_3 \end{bmatrix} \begin{bmatrix} a(\omega) \\ b(\omega) \\ c(\omega) \end{bmatrix} = \mathbf{M} \begin{bmatrix} a(\omega) \\ b(\omega) \\ c(\omega) \end{bmatrix}. \tag{6}$$

The vector of the coefficients on the right-hand side of Eq. (6) $[a(\omega)\, b(\omega)\, c(\omega)]^{\mathrm{T}}$ is obtained by inverting the matrix **M**. For example, the first element of coefficient vector is expressed in the following form:

$$a(\omega) = \frac{G_{11}(\omega)\sin 2k(x_2-x_3) - G_{22}(\omega)\sin 2k(x_1-x_3) + G_{33}(\omega)\sin 2k(x_1-x_2)}{\sin 2k(x_2-x_3) - \sin 2k(x_1-x_3) + \sin 2k(x_1-x_2)}. \tag{7a}$$

Using the notations of the microphone spacings $\Delta_a = x_2 - x_1$ and $\Delta_b = x_3 - x_2$, the total energy density proportional to $a(\omega)$ can be written as

$$E(\omega) = \frac{a(\omega)}{\rho_0 c^2} = \frac{G_{22}(\omega)\sin 2k(\Delta_a+\Delta_b) - G_{33}(\omega)\sin 2k\Delta_a - G_{11}(\omega)\sin 2k\Delta_b}{\rho_0 c^2(\sin 2k(\Delta_a+\Delta_b) - \sin 2k\Delta_a - \sin 2k\Delta_b)}. \tag{7b}$$

By expressing the position of the middle microphone as $\alpha = \Delta_a/(\Delta_a+\Delta_b)$, it is possible to examine how the denominator in Eq. (7b) changes with the non-dimensional variable $k(\Delta_a+\Delta_b)$ and the position of microphone 2 shown in Fig. 1. In Fig. 2 is shown the denominator in Eq. (7b) as a function of $k(\Delta_a+\Delta_b)$ and α. It is observed that when microphone 2 is positioned at the midpoint between microphones 1 and 3, i.e., $\Delta_a = \Delta_b$ and $\alpha = 0.5$, the denominator of Eq. (7b) has fewer poles that correspond to frequencies at which the energy density cannot be estimated. Thus in the following study, the case $\alpha = 0.5$ is considered. Substituting $\Delta = \Delta_a = \Delta_b$ in Eq. (7b) yields,

$$E(\omega) = \frac{a(\omega)}{\rho_0 c^2} = \frac{G_{11}(\omega) - 2G_{22}(\omega)\cos 2k\Delta + G_{33}(\omega)}{4\rho_0 c^2 \sin^2 k\Delta}. \tag{8}$$

Eq. (8) gives an estimate of the total energy density in a duct from measuring the sound pressure spectra of three equally spaced microphones. It is noted that in contrary to the finite-difference approximation method, Eq. (8) contains only the auto-spectral densities, thus no phase error occurs. When an inverse method is used, special attention should be paid to the propagation of measurement errors that can be amplified. A powerful technique for determining the uncertainty in the measured energy density is to calculate the variance of the estimation based on the uncertainty estimation of the different quantities and model parameters. The main systematic errors (amplitude calibration errors, sensor position errors and errors in the coefficients) as well as the statistical errors in the estimation of measured pressure spectra should be examined to verify that errors in some parameters do not amplify the errors in the final result. One of the objectives of this article is to show how it is possible to know *a priori* whether the precision of the method is acceptable for applications and what measurement parameters are to be chosen in order that the uncertainty of the estimate remains within fixed limits. The evaluation of uncertainties is made here in accordance with the recommendations of the GUM (Guide to the

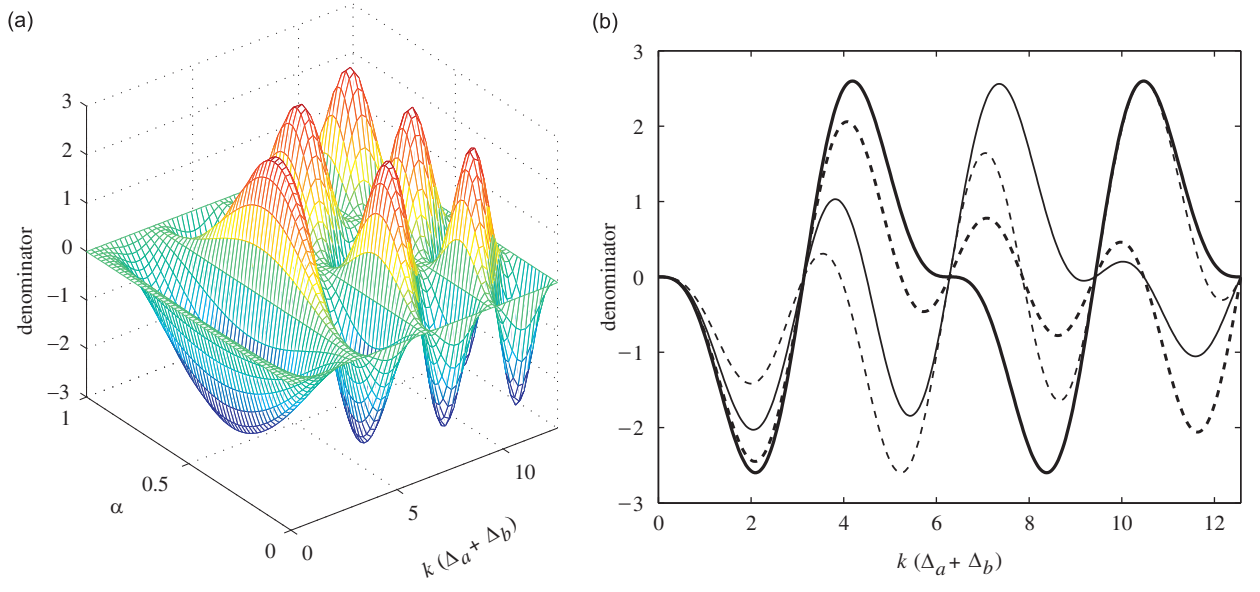

Fig. 2. Denominator of Eq. (7b) as a function of $k(\Delta_a+\Delta_b)$ and $\alpha = \Delta_a/(\Delta_a+\Delta_b)$, where Δ_a and Δ_b are shown in Fig. 1: (a) 3D view and (b) cross-section plots: thin dashed line $\alpha = 0.2$, thin solid line $\alpha = 0.3$, thick dashed line $\alpha = 0.4$ and thick solid line $\alpha = 0.5$.

expression of Uncertainty in Measurement [8,9]). A similar analysis was recently made for the determination of the uncertainty in the reflection coefficient by the two-microphone method [10].

The causes of measurement errors in the ducts can be numerous [11]. In this article, we distinguish two kinds of errors: one is the errors in auto-spectral density measurements including the errors in amplitude calibration and the statistical errors, the other is the parametric errors of the model related to the uncertainties that affect the vector of coefficients in Eq. (6) obtained by computing the inverse of the matrix **M**. It is supposed that the hypotheses of propagation model are satisfied. This physical model considers the propagation of plane waves in a non-dissipative fluid at rest inside a rigid wall duct of uniform cross-section. Thus discrepancies from the physical model are not considered in this analysis as sources of error.

3. Sensitivity to measurement errors

In this section two kinds of measurement errors are considered. One is the systematic errors due to calibration of the microphones; the other is the statistical errors of estimates for a random process.

3.1. Amplitude calibration errors

The errors in the microphone calibration have an influence on the estimate of the energy density by the three-microphone method. By introducing a coefficient s_i the measured auto-spectrum of each microphone can be expressed as $\overline{G}_{ii} = s_i\, G_{ii}$. The unknown coefficients s_i can be considered as Gaussian random variables of unit mean and normalized standard deviation ε_a. The random variables related to each microphone are independent of each other, so that the sensitivity of the estimate to errors of calibration can be presented by the following variance:

$$\mathrm{var}\{\overline{E}(s_1,s_2,s_3)\} \approx \sum_{i=1}^{3}\left(\frac{\partial E(\omega)}{\partial s_i}\right)^2 \mathrm{var}\{s_i\}. \tag{9}$$

Using the expression of Eq. (8) for E and considering that $\mathrm{var}\{s_i\} = \varepsilon_a^2$, Eq. (9) becomes

$$\mathrm{var}\{\overline{E}(\omega)\} \approx \varepsilon_a^2 \frac{G_{11}^2(\omega) + 4G_{22}^2(\omega)\cos^2 2k\Delta + G_{33}^2(\omega)}{16(\rho_0 c^2)^2 \sin^4 k\Delta}. \tag{10}$$

The factor of sensitivity S_a to errors of calibration is defined as the ratio $S_a = \varepsilon\{\overline{E}\}/\varepsilon_a$ of the normalized standard deviation $\varepsilon\{\overline{E}(\omega)\} = \sqrt{\mathrm{var}\{\overline{E}(\omega)\}}/E(\omega)$ to the normalized standard deviation of the calibration uncertainty ε_a. To evaluate the significance of S_a, the power spectral densities in Eq. (10) are replaced by their expressions (5a) and the total energy density Eq. (8) is used. In Fig. 3 is shown the factor of sensitivity S_a as a function of a non-dimensional position $2kx+\varphi$ in the partial standing wave. φ is an unknown phase shift that depends on several factors including the phase between the two opposite waves. The curves shown in Fig. 3 correspond to three values of the ratio $r^2 = G_{BB}/G_{AA}$ of the PSD of the two opposite waves ($r^2 = 1,\ 0.25$ and 0), for four sets of values of $k\Delta$ (1 and 2.5) and γ_{AB}^2 (1 and 0.5). It is noted that the factor of sensitivity varies as the function of the position in the quasi-stationary wave. As this position cannot be known, the maximum factor of sensitivity $S_{a\,\max}$ is introduced, which is the ratio of the maximum normalized standard deviation on a variation of $2kx$ over 2π to the normalized standard deviation of the calibration errors ε_a, i.e., $S_{a\,\max} = \varepsilon_{\max}\{\overline{E}\}/\varepsilon_a$. Fig. 4 shows $S_{a\,\max}$ as a function of $k\Delta$ for three values of the ratio $r^2 = G_{BB}/G_{AA}$ and by varying the coherence between the two

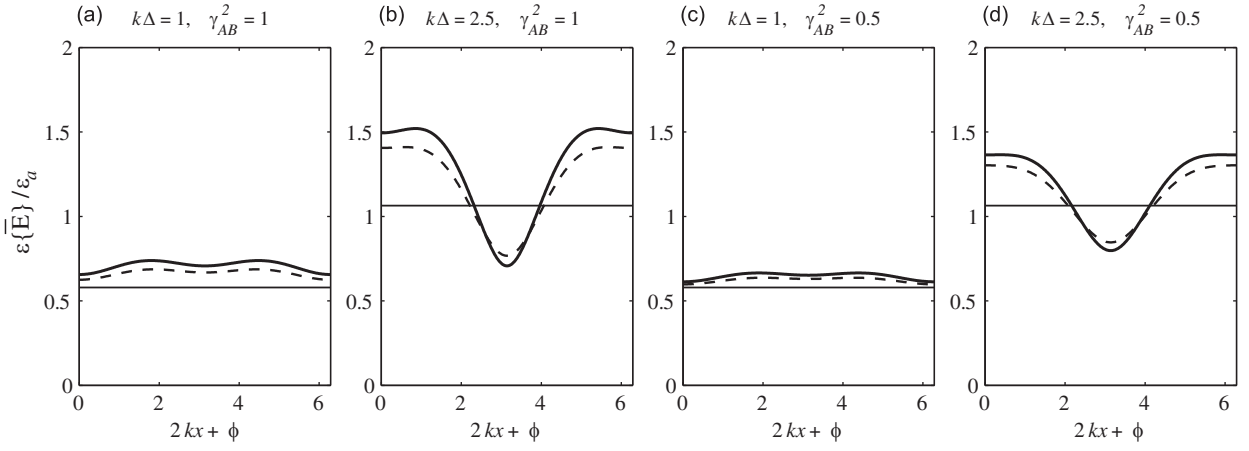

Fig. 3. Factor of sensitivity to the errors of calibration $S_a = \varepsilon\{\overline{E}\}/\varepsilon_a$ as a function of $2kx+\varphi$ for $r^2=1$ (thick solid line), $r^2=0.25$ (dashed line) and $r^2=0$ (thin solid line), for four sets of values of parameters $k\Delta$ and γ_{AB}^2, (a)–(d).

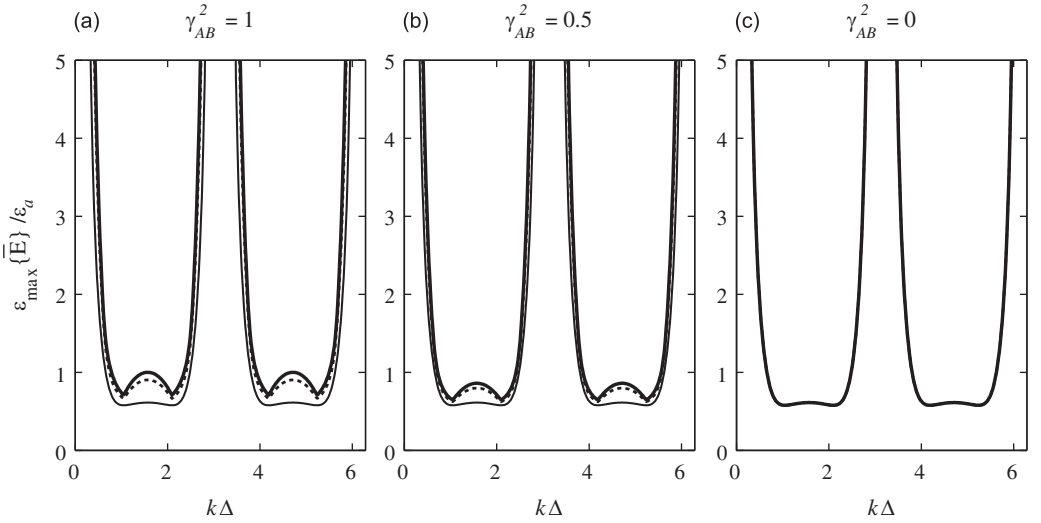

Fig. 4. Maximum factor of sensitivity $S_{a\,\max} = \varepsilon_{\max}\{\bar{E}\}/\varepsilon_a$ related to the uncertainty of calibration versus $k\Delta$ for $r^2=1$ (thick solid line), $r^2=0.25$ (dashed line) and $r^2=0$ (thin solid line), for different values of γ_{AB}^2, (a)–(c).

opposite waves γ_{AB}^2. The maximum value of the normalized standard deviation is neither very sensitive to the coherence between the two opposite waves γ_{AB}^2 nor to their amplitude ratio r^2. The large values are found around the zeroes of the function $\sin k\Delta$ (denominator of Eq. (8)). Similar problems occur in the measurement of sound intensity in duct with two microphones [12]. Thus the error representations are associated with a π periodicity. Consider the following example for determining the maximum factor of sensitivity. If the normalized standard deviation of the uncertainty of calibration ε_a is of the order of magnitude 5% (that is, approximately ± 0.22 dB) and if one wants the normalized standard deviation of the energy density lower than 20% [-0.97 dB, $+0.79$ dB], then the usable frequency range will be those corresponding to the values of the maximum factor of sensitivity $S_{a\,\max} = \varepsilon_{\max}\{\bar{E}\}/\varepsilon_a < 0.20/0.05 = 4$, i.e., in a frequency range where $k\Delta$ is between $n\pi \pm 0.48$ ($n=0, 1, 2\ldots$). The calibration is generally made using a pistonphone calibrator and the quantity $G_{ii}(\omega)/(\rho_0 c)$ is concerned; thus, it is not necessary to consider uncertainties in $\rho_0 c$ on errors related to the speed of sound.

3.2. Statistical errors

In the case of the measurement of random signals, the finite duration of analysis leads to errors in estimation of the spectral densities. The variance of these statistical errors can be given by

$$\mathrm{var}\left\{\hat{E}(G_{11},G_{22},G_{33})\right\} \approx \sum_{i}^{3}\sum_{j}^{3}\frac{\partial E}{\partial G_{ii}}\frac{\partial E}{\partial G_{jj}}\mathrm{cov}\left\{\hat{G}_{ii},\hat{G}_{jj}\right\}, \tag{11}$$

where the covariance of the auto-spectral density for Gaussian processes is

$$\mathrm{cov}\left\{\hat{G}_{ii}(\omega),\hat{G}_{jj}(\omega)\right\} \approx \frac{|G_{ij}(\omega)|^2}{n} = \frac{\gamma_{ij}^2(\omega)G_{ii}(\omega)G_{jj}(\omega)}{n}, \tag{12a}$$

and

$$\mathrm{cov}\left\{\hat{G}_{ii}(\omega),\hat{G}_{ii}(\omega)\right\} = \mathrm{var}\left\{\hat{G}_{ii}(\omega)\right\} \approx \frac{G_{ii}^2(\omega)}{n}, \tag{12b}$$

where n is the number of the Fourier transform of segments of digital signals (periodograms) averaged to estimate the PSD. These expressions for the variance of the spectral density are due to Jenkins and Watt [13] and are likely to provide good estimates using the measured spectral densities in Eq. (12) (see, for example, Refs. [3,14–16]). They can be used for random signals like white or colored noises. These variance expressions assume that the periodograms are independent, which means that a rectangular window is used without overlap (Bartlett's procedure). The variance of the PSD estimated using a window is approximately the same as that for the Bartlett's procedure: the decrease of the effective duration of each segment is compensated by the increase of the effective width of each spectral bin. Welch [17] has introduced a modification of the Bartlett's procedure using window and overlap. When the segments overlap each other, the modified periodograms are not independent. A multiplying factor [17,18] using the normalized correlation function $C(\tau)$ of the window approximates the variance of the modified periodogram for an overlap period. For an overlap of 50%, the multiplying factor is $1+2C^2(L\Delta t/2)$, where $L\Delta t$ is the length of the window (Δt is the sampling interval). With the Hanning window, the value of the normalized correlation function is $C(L\Delta t/2) \cong 0.167$, the multiplying factor is 1.056, but the

average number n is doubled for the same length of signal. This leads to a reduction in the variance by 1.056/2, thus Eqs. (12a)–(12b) can always be used with the appropriate average number.

Using the expression for the energy density (Eq. (8)) and making some manipulations, one obtains

$$\mathrm{var}\left\{\hat{E}(\omega)\right\} \approx \frac{1}{n}\frac{G_{11}^2(\omega)+4G_{22}^2(\omega)\cos^2 2k\Delta+G_{33}^2(\omega)}{16(\rho_0 c^2)^2\sin^4 k\Delta}+\frac{1}{n}\frac{|G_{31}(\omega)|^2-2|G_{21}(\omega)|^2\cos 2k\Delta-2|G_{32}(\omega)|^2\cos 2k\Delta}{8(\rho_0 c^2)^2\sin^4 k\Delta}. \tag{13}$$

The first part on the right-hand side of Eq. (13) corresponds to independent measurements that ignore the covariance terms. The second part, which comes from the covariance terms of Eq. (11) for dependent measurements, includes cross-spectra and depends on the coherence functions between the microphone signals. Even though the cross-power spectral densities between sensors are not measured, the coherence functions have influence on the precision of the results when the signals from the sensors are acquired simultaneously. The coherence functions are practically never equal to zero [4], even if the two waves traveling in opposite directions are uncorrelated ($\gamma_{AB}^2=0$). The only configuration where the second part on the right-hand side of Eq. (13) does not exist is when measurements of pressure are carried out successively (thus independently), which results in null covariance. On the contrary, the second term will be taken into account when measurements are carried out simultaneously. To evaluate the variance of energy density due to statistical errors, similarly to Eq. (5a) the cross-spectral densities in Eq. (13) are represented by

$$G_{ij}(\omega)=G_{AA}(\omega)e^{\mathrm{j}k(x_i-x_j)}+G_{BB}(\omega)e^{-\mathrm{j}k(x_i-x_j)}+2|G_{AB}(\omega)|\cos(k(x_i+x_j)+\varphi(\omega)). \tag{14}$$

The square of the absolute value of $G_{ij}(\omega)$ is given by

$$|G_{ij}(\omega)|^2=[(G_{AA}(\omega)+G_{BB}(\omega))\cos k(x_i-x_j)+2|G_{AB}(\omega)|\cos(k(x_i+x_j)+\varphi(\omega))]^2+[(G_{AA}(\omega)-G_{BB}(\omega))\sin k(x_i-x_j)]^2, \tag{15a}$$

and

$$|G_{ij}(\omega)|^2=[a(\omega)\cos k(x_i-x_j)+b(\omega)\cos k(x_i+x_j)-c(\omega)\sin k(x_i+x_j)]^2+[d(\omega)\sin k(x_i-x_j)]^2 \tag{15b}$$

where $a(\omega)$, $b(\omega)$ and $c(\omega)$ have the same definitions as those in Eq. (5b) and $d(\omega)=G_{AA}(\omega)-G_{BB}(\omega)$ is proportional to the active sound intensity in the duct [4].

Using Eqs. (13), (15a), (4) and introducing the ratio $r^2=G_{BB}/G_{AA}$ of the opposite waves, the normalized standard deviation of the statistical errors $S_r=\varepsilon\{\hat{E}(\omega)\}\sqrt{n}=\sqrt{n\mathrm{var}\{\hat{E}(\omega)\}}/E(\omega)$ is written as

$$S_r=\frac{\sqrt{n\mathrm{var}\{\hat{E}(\omega)\}}}{E(\omega)}\approx\frac{\sqrt{1+r^4(\omega)+2\gamma_{AB}^2(\omega)r^2(\omega)}}{1+r^2(\omega)}. \tag{16}$$

These errors have the particularity of being independent of the microphone positions with respect to the standing wave (consequently $S_{r\,\max}=\max\{S_r\}=S_r$). They are also independent of the microphone spacing, thus independent of the dimensionless variable $k\Delta$. The highest value $S_r=1$ corresponds to two coherent opposite waves ($\gamma_{AB}^2=1$), in accordance with the results in Ref. [4]. Fig. 5 shows the normalized standard deviation of the statistical errors $S_r=\varepsilon\{\hat{E}(\omega)\}\sqrt{n}$ versus the coherence function γ_{AB}^2 for four values of the square amplitude ratio r^2.

In Eqs. (13) and (16), it is considered that the signals are acquired simultaneously (multi-channel acquisition). If one-channel analyzer is used, the auto-power spectral densities are obtained successively, therefore independently, so that the terms of covariance (i.e., the second part on the right-hand side of Eq. (13)) do not appear in the variance of the statistical error in E. In this case, instead of using the two parts on the right-hand side of Eq. (13), the statistical error presents the variations when the quasi-stationary wave moves with respect to the microphone positions, similarly to that shown in Fig. 3. The statistical errors in the two situations are shown in Fig. 6 by the maximum factor of sensitivity $S_{r\,\max}$ for four

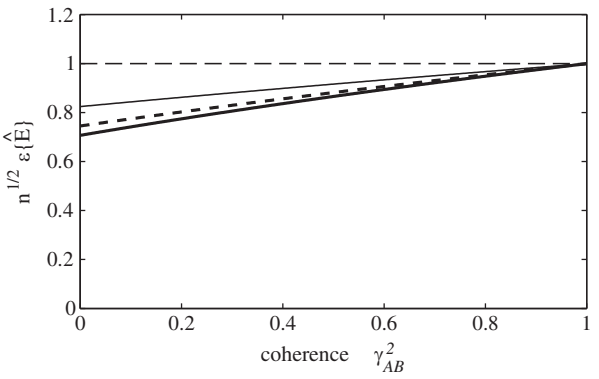

Fig. 5. Normalized standard deviation of the statistical errors with simultaneous acquisitions versus the coherence function γ_{AB}^2, for square amplitude ratio $r^2=1$ (thick solid line), $r^2=0.5$ (thick dashed line), $r^2=0.25$ (thin solid line) and $r^2=0$ (thin dashed line).

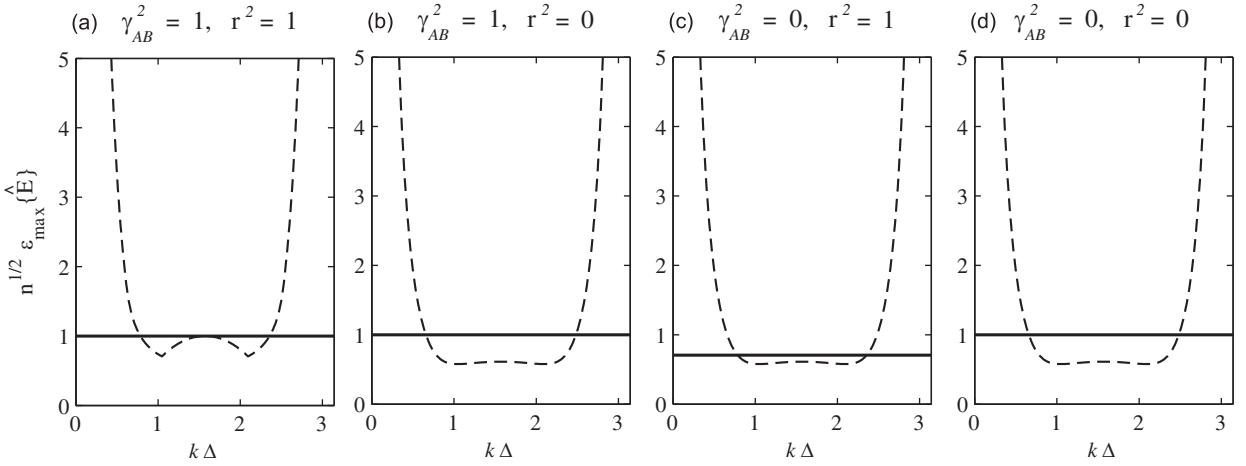

Fig. 6. Maximum value of the factor of sensitivity to the statistical errors for simultaneous (solid line) and successive (dashed line) measurements by the three microphones. It is presented as a function of $k\Delta$ for four sets of values of γ_{AB}^2 and $r^2 = G_{BB}/G_{AA}$, (a)–(d).

configurations of field: for both coherent opposite waves ($\gamma_{AB}^2 = 1$) and incoherent waves ($\gamma_{AB}^2 = 0$) at the two amplitude ratios $r = 1$ and 0.

4. Sensitivity to the parametric errors of model

4.1. Errors due to uncertainty in the position of the sensors

In general, the microphones are accurately mounted in the duct with flush diaphragm. Positioning the microphones is not easy when air flow exists, which requires that nose cones are added to the microphones. To take the error due to position of the sensors into account, we consider the microphone positions x_i as Gaussian random variables centered on the nominal values. These random variables are independent for the three positions but their standard deviation is identical and is noted by σ_x. The variance of these errors can thus be expressed, without the use of cross terms, by

$$\mathrm{var}\left\{\tilde{E}(x_1,x_2,x_3)\right\} \approx \sigma_x^2 \sum_{i=1}^{3} \left(\frac{\partial E(\omega)}{\partial x_i}\right)^2. \tag{17}$$

By the use of Eq. (8), the derivatives of the total energy with respect to the microphone positions x_i are given by

$$\frac{\partial E(\omega)}{\partial x_1} = -k\frac{2G_{22}(\omega)(\cos 2k\Delta+1)-G_{11}(\omega)(2\cos 2k\Delta+1)-G_{33}(\omega)}{4\rho_0 c^2 \sin 2k\Delta \sin^2 k\Delta}, \tag{18a}$$

$$\frac{\partial E(\omega)}{\partial x_2} = k\frac{2(G_{33}(\omega)-G_{11}(\omega))\cos 2k\Delta}{4\rho_0 c^2 \sin 2k\Delta \sin^2 k\Delta}, \tag{18b}$$

$$\frac{\partial E(\omega)}{\partial x_3} = k\frac{2G_{22}(\omega)(\cos 2k\Delta+1)-G_{33}(\omega)(2\cos 2k\Delta+1)-G_{11}(\omega)}{4\rho_0 c^2 \sin 2k\Delta \sin^2 k\Delta}. \tag{18c}$$

It is shown that it is interesting to use the normalized standard deviation of the position σ_x/Δ for factorizing $k\Delta$ and to express the uncertainty as a function of the non-dimensional frequency, as for the calibration errors. Fig. 7 shows the factor of sensitivity $S_x = \varepsilon\{\tilde{E}(\omega)\}/(\sigma_x/\Delta)$, the ratio of the normalized standard deviation of the energy density defined by $\varepsilon\{\tilde{E}(\omega)\} = \sqrt{\mathrm{var}\{\tilde{E}(\omega)\}}/E(\omega)$ to the normalized standard deviation σ_x/Δ as a function of $2kx+\varphi$. The curves in Fig. 7 show the fluctuations of the factor of sensitivity as a function of the microphone positions with respect to the standing wave. The standard deviation takes naturally smaller values when the ratio of the amplitudes of the two opposite waves decreases, until it vanishes for a single wave ($r^2 = 0$). It is also noticed that the reduction of the coherence between the opposite waves results in the decrease of the amplitude of the stationary field. Like the errors due to calibration, we consider the maximum uncertainty over a half-wavelength. Fig. 8 shows the factor of maximum sensitivity to the errors of microphone positions $S_{x\max}$ defined as the maximum normalized standard deviation $\varepsilon_{\max}\{\tilde{E}\}$ normalized with respect to σ_x/Δ. A significant increase in the uncertainties was found when the non-dimensional frequencies are around $k\Delta = m\pi$ ($m = 0,1,2,\ldots$), but also a linear increase with $k\Delta$, i.e., when the wavelength decreases. Whereas the uncertainty of measurement does not provide any frequency limit (except the frequencies close to the poles), the uncertainty related to the microphone positions will result in giving a maximum value for $k\Delta$. Thus, if the uncertainty in the most unfavorable

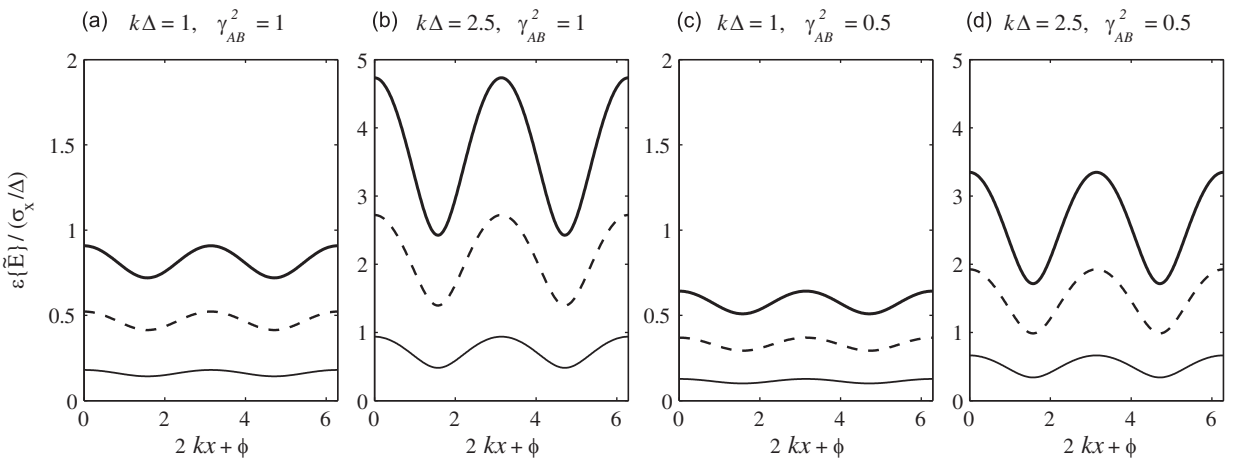

Fig. 7. Factor of sensitivity S_x related to errors of microphone positions as a function of $2kx+\varphi$ for $r^2=1$ (thick solid line), $r^2=0.1$ (dashed line) and $r^2=0.01$ (thin solid line), for four sets of values of parameters $k\Delta$ and γ_{AB}^2, (a)–(d).

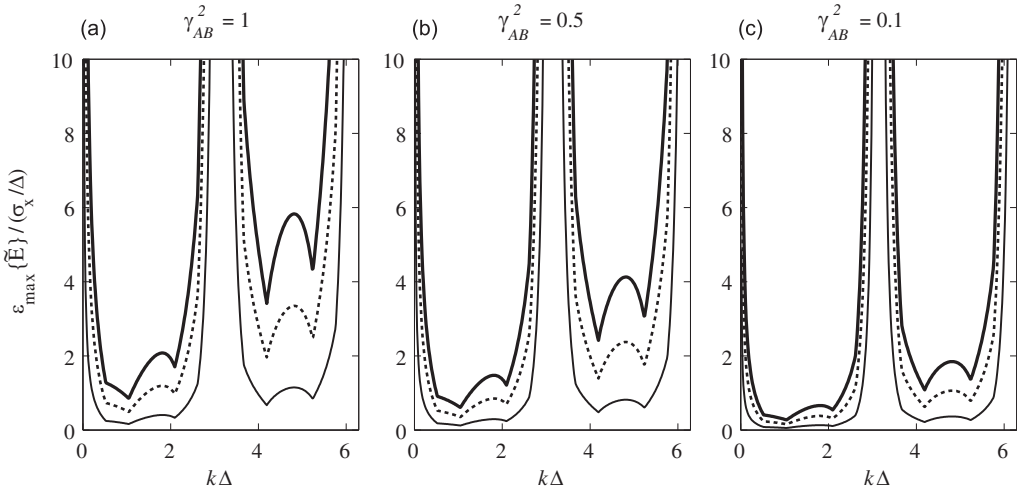

Fig. 8. Factor of maximum sensitivity $S_{x\max}$ related to the uncertainty in the microphone positions (maximal normalized deviation over σ_x/Δ) versus $k\Delta$ for $r^2=1$ (thick solid line), $r^2=0.25$ (dashed line) and $r^2=0$ (thin solid line), for three values of γ_{AB}^2, (a)–(c).

case ($\gamma_{AB}^2=1$, $r^2=1$) should not be higher than that of the calibration, it is necessary to limit the frequency band to $k\Delta<\pi$, for a normalized standard deviation σ_x/Δ typically ranging between 1% and 5%. In practice, this upper frequency limit will be chosen less than or equal to the frequency limit imposed by the plane wave model and specified in Section 2.

4.2. Errors due to uncertainty related to the speed of sound

The discrete spectral components corresponding to the estimate of the PSD are well located on the frequency axis by the FFT analysis. On the other hand, the model does not depend directly on the frequency but on the wavenumber $k=2\pi f/c$, which is related to the frequency by the speed of sound. It is thus advisable to examine the sensitivity introduced by uncertain knowledge of the speed of sound (with a normalized standard deviation ε_c). The related variance is given by

$$\mathrm{var}\left\{\check{E}(c)\right\} \approx c^2\varepsilon_c^2\left(\frac{\partial E(\omega)}{\partial c}\right)^2, \tag{19}$$

and the normalized standard deviation of the energy density is

$$\varepsilon\left\{\check{E}(\omega)\right\} = \frac{\sqrt{\mathrm{var}\{\check{E}(c)\}}}{E(\omega)} \approx \varepsilon_c\left|2k\Delta\,\frac{\cos k\Delta(G_{11}(\omega)-2G_{22}(\omega)+G_{33}(\omega))}{\sin k\Delta(G_{11}(\omega)-2G_{22}(\omega)\cos 2k\Delta+G_{33}(\omega))}-1\right|. \tag{20}$$

According to the analysis of calibration errors (Section 3.1) that concern the quantities $G_{ii}/\rho_0 c$, the normalized standard deviation of Eq. (20) corresponds to $\varepsilon\{\check{E}(c)\}\equiv\varepsilon\{\rho_0 cE(c)\}$. Using Eq. (20) and the model of field given by Eq. (5a), the factor of

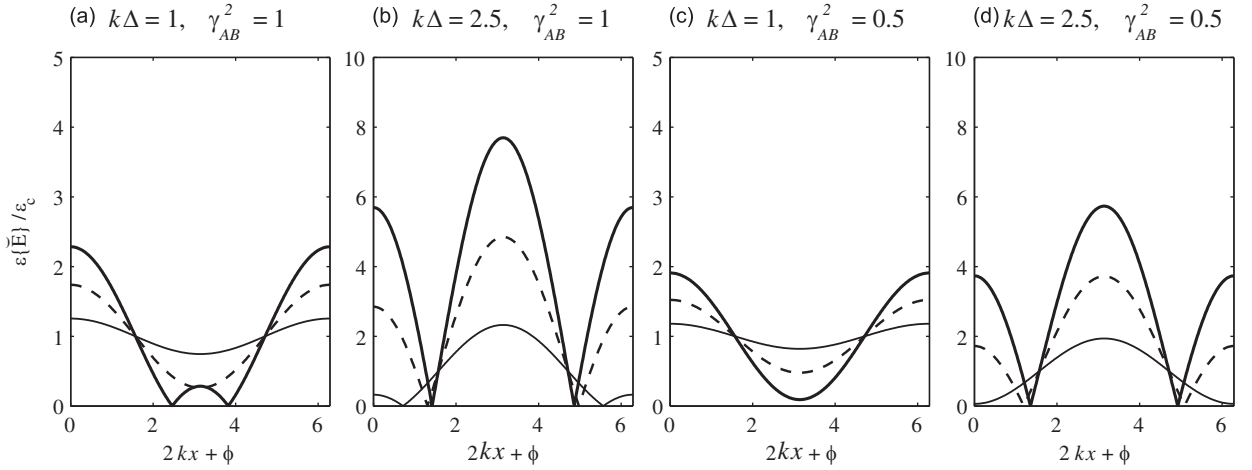

Fig. 9. Factor of sensitivity S_c related to errors in the speed of sound $S_c = \varepsilon\{\check{E}\}/\varepsilon_c$ as a function of $2kx+\varphi$ for $r^2=1$ (thick solid line), $r^2=0.25$ (dashed line) and $r^2=0$ (thin solid line), for four sets of values of parameters $k\Delta$ and γ_{AB}^2, (a)–(d).

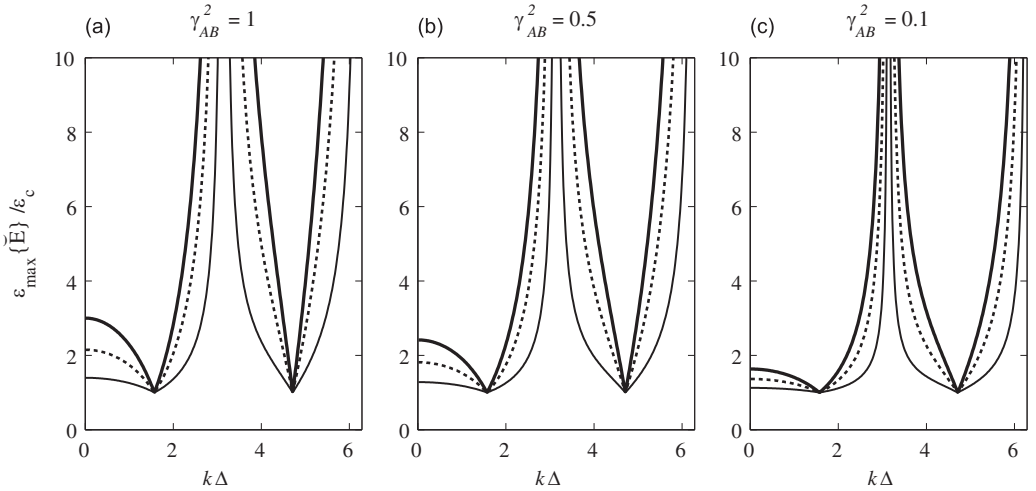

Fig. 10. Maximum factors of sensitivity $S_{c\,\max}$ related to the uncertainty in the speed of sound ($S_{c\,\max} = \varepsilon_{\max}\{\check{E}\}/\varepsilon_c$) versus $k\Delta$ for $r^2=1$ (thick solid line), $r^2=0.1$ (dashed line) and $r^2=0.01$ (thin solid line), for three values of γ_{AB}^2, (a)–(c).

sensitivity $S_c = \varepsilon\{\check{E}(\omega)\}/\varepsilon_c$ is calculated and shown in Fig. 9 as a function of $2kx+\varphi$. Similar to the expression for $S_{x\,\max}$, the maximum values in a range of a half-wavelength allow one to express the maximum factor of sensitivity to uncertainty in the speed of sound as $S_{c\,\max} = \varepsilon_{\max}\{\check{E}\}/\varepsilon_c$. The results are shown in Fig. 10. From these results it is demonstrated that an increase occurs around $k\Delta = m\pi$ $(m = 1,2,\ldots)$. However the uncertainty in the speed of sound often depends on uncertainty in the temperature. Since the speed of sound in a gas can be expressed as a function of the absolute temperature T_K by $c = \sqrt{\gamma R T_K}$ (γ is the ratio of specific heats and $R = R_*/M$, where $R_* \approx 8.3145$ in J mol^{-1} K^{-1} is the molar gas constant and M the mean molar mass in kilogram per mole) the normalized standard deviation of the speed of sound is thus given by

$$\varepsilon_c \approx \frac{1}{c}\frac{\partial c}{\partial T_K}\sigma_T = \frac{\sigma_T}{2T_K}, \tag{21}$$

where σ_T is the standard deviation of the absolute temperature. Thus if the temperature in the fluid is 30 °C ($T_K \cong 303$ K) and the uncertainty during the test is 3 °C ($\sigma_T = 3$ K), σ_T/T_K is approximately 1% and the normalized standard deviation of the speed of sound is approximately 0.5%.

5. Discussion

The principal causes of uncertainty due to unknown errors in the various measurement parameters have been treated like uncertainties. These uncertainties in the calibration of the microphones, the position of the sensors, the knowledge of the speed of sound and the estimate of the PSD of acoustic pressures are shown by the factors of sensitivity denoted,

respectively, by $S_{a\,\max}$, $S_{x\,\max}$, $S_{c\,\max}$ and $S_{r\,\max}$, obtained from the maximum values of the standard deviations in a range of a half-wavelength. These factors of sensitivity have been shown as a function of non-dimensional frequency $k\Delta$ in Figs. 4, 6, 8 and 10. The parameters of the general model of plane wave in a duct such as the coherence between the opposite waves γ^2_{AB} and the ratio of amplitudes r have influence on these factors. In Fig. 11 is shown the four factors of sensitivity for the case where $\gamma^2_{AB}=1$ and $r^2=1$, which is the hardest configuration for the acoustic fields.

Total uncertainty in the estimate of the energy density E is obtained by summing the variances of all independent sources of uncertainties, so that the standard deviation of E is expressed as

$$\varepsilon\{E(\omega)\} \approx \sqrt{\varepsilon_a^2 S_a^2 + \frac{1}{n} S_r^2 + \frac{\sigma_x^2}{\Delta^2} S_x^2 + \varepsilon_c^2 S_c^2}. \tag{22}$$

The variables in Eq. (22) are the same as those we defined previously. Like all of the factors of sensitivity that fluctuate in terms of the unknown microphone positions with respect to the quasi-stationary wave, $\varepsilon_{\max}\{E(\omega)\}$ is defined as the maximum value of $\varepsilon\{E(\omega)\}$ in the interval $0 \le 2kx+\varphi \le \pi$ and is written as

$$\varepsilon_{\max}\{E(\omega)\} \le \sqrt{\varepsilon_a^2 S_{a\,\max}^2 + \frac{1}{n} S_{r\,\max}^2 + \frac{\sigma_x^2}{\Delta^2} S_{x\,\max}^2 + \varepsilon_c^2 S_{c\,\max}^2}. \tag{23}$$

It is evident that $\varepsilon_{\max}\{E(\omega)\}$ is even raised by considering the maximum factors of sensitivity to the various sources of error.

To adjust the measurement parameters, a strategy can consist of using Eq. (23) and selecting the parameters in order to keep (i) the term related to the error of calibration, (ii) the term corresponding to the statistical errors and (iii) the sum of the two terms of the errors of model (microphone positions and speed of sound) to be the same order of magnitude. For instance, for $\varepsilon_{\max}\{E\}=26\%$, which corresponds to $10\log_{10}(1\pm\varepsilon\{E\})=[-1.3\text{ dB}, +1\text{ dB}]$, the minimum and maximum values of the non-dimensional frequency $k\Delta$ are required so that the factor of sensitivity $S_{a\,\max}$ is lower than $0.26/0.05/\sqrt{3}=3$ (5% being the normalized standard deviation of uncertainty in the calibration of the microphones, i.e., ± 0.2 dB). This useful frequency band (expressed in terms of the non-dimensional frequency) has two bounds of values $k_{\min}\Delta \approx 0.519$ and $k_{\max}\Delta \approx 2.623$, as indicated in Fig. 11. The minimal number of acquisitions used to obtain the average auto-spectrum is calculated by $n = S_{r\,\max}^2/\varepsilon^2\{\hat{E}\} = S_{r\,\max}^2/(0.26/\sqrt{3})^2$. The value of the factor of sensitivity is $S_{r\,\max}=1$ over all the frequency range for simultaneous measurements, which corresponds to approximately 45 acquisitions (and nearly 400 for successive measurements with $S_{r\,\max}=3$ at the bounds of the range). At the bounds of the frequency band, the maximum factor of sensitivity to the position errors of the microphones $S_{x\,\max}$ has the values 1.31 and 6.65. It is thus necessary that the normalized error σ_x/Δ be lower than $0.26/\sqrt{6}/6.65 \approx 0.016$ (1.6%). This condition can generally be satisfied. If, for some practical reasons, the microphones cannot be positioned with a sufficient precision, the measurement of microphone spacing, however, will be more precise. It is then enough to substitute Eq. (7b) for Eq. (8) and take the standard deviation of the measurement of position to evaluate σ_x/Δ. For the maximum factor of sensitivity to the errors in the speed of sound, the limits of the frequency band (Fig. 11) are 2.82 and 10.19, which leads to imposing ε_c on a value lower than $0.26/\sqrt{6}/10.19 \approx 0.010$ (1%). Thus, a measuring range of $\log_2(k_{\max}\Delta/k_{\min}\Delta) \approx 2.3$ octaves makes it possible to guarantee a standard deviation of uncertainties within the interval $[-1.3+1]$ dB by carrying out 50 independent acquisitions, with a calibration accuracy of ± 0.2 dB, a relative uncertainty of 1.6% for the microphone spacing Δ and 1% for the speed of sound. If the maximal frequency has to be 2000 Hz, the microphone spacing is thus $\Delta = (k_{\max}\Delta)c/(2\pi f_{\max}) \approx 0.072$ m and the minimum frequency is $f_{\min} = (k_{\min}\Delta)c/(2\pi\Delta) \approx 395$ Hz. Simultaneous measurements using three channel acquisitions lead

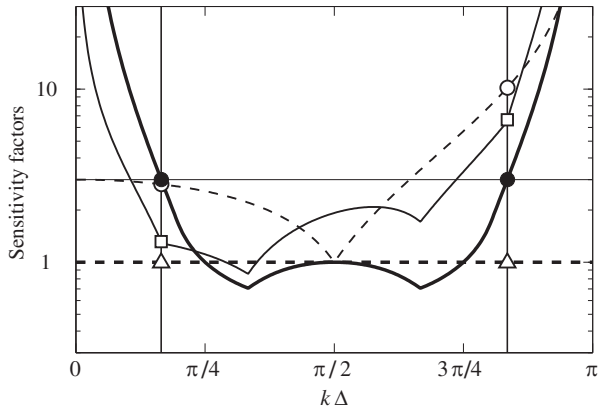

Fig. 11. Maximum values of the sensitivity factor when $\gamma^2_{AB}=1$ and $r^2=1$, versus $k\Delta$ for the error of calibration $S_{a\,\max}$ (thick solid line), error of the microphone positions $S_{x\,\max}$ (thin solid line), error in the speed of sound $S_{c\,\max}$ (thin dashed line) and the statistical errors for the simultaneous measurements $S_{r\,\max}$ (thick dashed line).

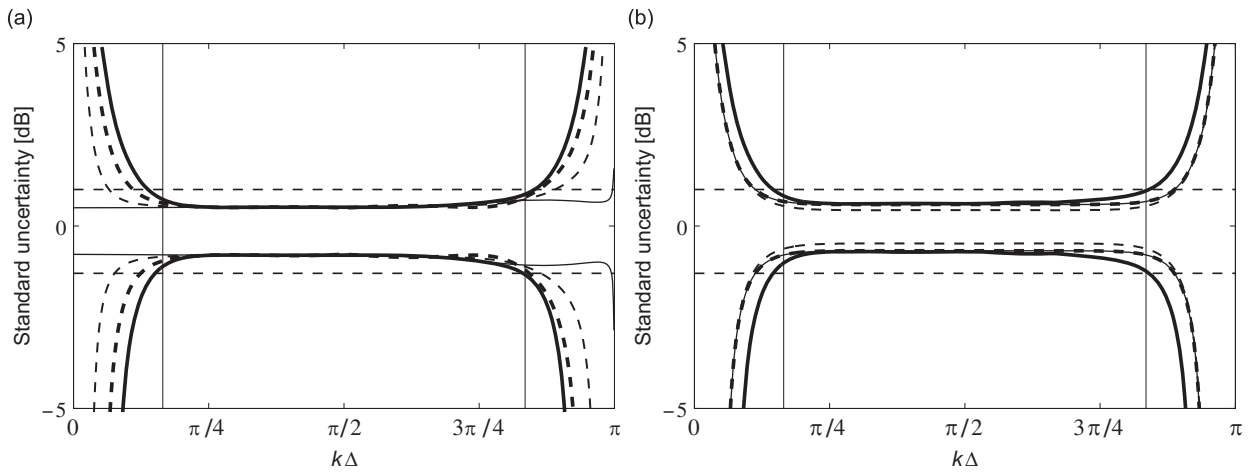

Fig. 12. Confidence intervals corresponding to uncertainty in the energy density (the vertical and horizontal lines correspond to the frequency limits defined in the text and the objectives of −1.3 dB and +1 dB). (a) $\varepsilon\{E\}$ when $\gamma_{AB}^2=1$ and $r^2=1$ for $2kx+\varphi=0$ (thick solid line), $2kx+\varphi=\pi/2$ (thick dashed line), $2kx+\varphi=3\pi/4$ (thin dashed line) and $2kx+\varphi=\pi$ (thin solid line). (b) $\varepsilon_{\max}\{E\}$ for $\gamma_{AB}^2=1$, $r^2=1$ (thick solid line), $\gamma_{AB}^2=1$, $r^2=0$ (thick dashed line), $\gamma_{AB}^2=0$, $r^2=1$ (thin dashed line) and $\gamma_{AB}^2=0.5$, $r^2=0.5$ (thin solid line).

to statistical errors independent of both the position in the quasi-stationary wave and the normalized frequency $k\Delta$. However, the uncertainty analysis also shows that successive measurements with a one-channel analyzer can be achieved without significant loss of accuracy if the source remains perfectly stationary during the measurement and the number of independent acquisitions is increased to 400.

This example shows how to choose the parameters of measurement to maintain *a priori* the uncertainties below a fixed limit, by considering the most unfavorable case (maximum value over $2kx+\varphi$ when $\gamma_{AB}^2=1$ and $r^2=1$). With the same estimates of uncertainties in the measured quantities and the model parameters, the estimate of uncertainty in the energy density is calculated using Eq. (22). In Fig. 12 is shown the confidence intervals in dB obtained by $10\log(1\pm\varepsilon\{E\})$.

Fig. 12a shows the comparison between $\varepsilon_{\max}\{E(\omega)\}$ (the most unfavorable case where $\gamma_{AB}^2=1$ and $r^2=1$) and $\varepsilon\{E(\omega)\}$ calculated for various values of $2kx+\varphi$ corresponding to the positions of the standing wave with respect to the microphone positions. It is possible to verify that the uncertainty intervals are bounded by those that use $\varepsilon_{\max}\{E\}$. In Fig. 12b is shown $\varepsilon_{\max}\{E(\omega)\}$ calculated from Eq. (22) for several characteristics of the sound field in the duct, i.e., for different sets of the values of γ_{AB}^2 and r^2. The upper bound given by Eq. (23) can limit the measurement uncertainty and ensure the operating range of the proposed method, despite no knowledge of microphone positions in the quasi-stationary pressure field, the coherence and amplitude ratio of the opposite waves.

In this analysis, uncertainties in the various parameters were modeled as Gaussian random variables. It can be fully justified for the uncertainty in the microphone positions around their nominal value. It is a valid approximation for the statistical errors of the auto-spectrum insofar as the number of averages is sufficiently large so that the normalized standard deviation is much lower than 1. If the dissipation or a weak flow was suspected, the wavenumbers of the two waves traveling in opposite directions described by Eq. (1) are different and given by $k_{\pm}=(2\pi f/c)(1-\mathrm{j}\delta)/(1\pm M)$ [12] and the uncertainties in terms of dissipation δ and Mach number M must be taken into account. As the existence and magnitude of these effects are difficult to know in practice, these parameters can be modeled as random variables with a positive mathematical expectation $(0,+\infty)$. The probability density of the random variables is obtained using the principle of maximum entropy as suggested in Ref. [19]. In the case where the flow is stronger, the model of propagation should be revised. As a result the expressions for the energy densities must be reformulated [20].

6. Conclusion

The total energy density is a useful quantity to describe the sound field in the region between two discontinuities in a duct because it is independent of the microphone position. This study has shown that a three-microphone method, which is based on the inversion of a general model of partially coherent plane waves traveling in opposite directions, allows the energy density to be obtained without taking the phase between microphones into account. The robustness of this method has been verified by calculating the sensitivity to the four principal sources of statistical errors (position of the microphones and speed of sound, calibration and fluctuation of the random signal). The total uncertainty expressed by the normalized standard deviation is used to select the measurement parameters and to define a range of frequency guaranteed by a given confidence interval. This approach makes it possible to provide the uncertainty intervals of the measurement.

References

[1] G.W. Elko, Frequency Domain Estimation of the Complex Acoustic Intensity and Acoustic Energy Density, PhD Thesis, Pennsylvania State University, State College, USA, 1984.
[2] B.S. Cazzolato, C.H. Hansen, Errors in the measurement of acoustic energy density in one-dimensional sound fields, *Journal of Sound and Vibration* 236 (3) (2000) 801–831.
[3] J. Ghan, B.S. Cazzolato, S.D. Snyder, Statistical errors in the estimation of time-averaged acoustic energy density using the two-microphone method, *Journal of the Acoustical Society of America* 115 (2004) 1179–1184.
[4] J.-C. Pascal, J.-H. Thomas, J.-F. Li, On the statistical errors of acoustic energy densities estimate using two microphones, *Journal of the Acoustical Society of America* 124 (4) (2008) 2085–2089.
[5] F. Jacobsen, A note on finite difference estimation of acoustic particle velocity, *Journal of Sound and Vibration* 256 (2002) 849–859.
[6] F.J. Fahy, *Sound Intensity*, second ed.,E & FN Spon, 1995.
[7] J.-L. Trolle, E. Luzzato, Application of structural intensity for diagnostic in one dimension problems, *Proceedings of the Third International Congress on Intensity Techniques*, Senlis (France), 27–29 August 1990, pp. 397–404.
[8] ISO, *GUM—Guide to the Expression of Uncertainty in Measurement*, International Organization for Standardization, 1995.
[9] M. Priel, The approaches for measurement uncertainties evaluation, *Proceedings of the Symposium on Managing Uncertainties in Noise Measurements and Predictions*, Le Mans (France), 27–29 June 2005, CD paper 005, p. 8.
[10] T. Schultz, M. Sheplak, L.N. Cattafesta III, Uncertainty analysis of the two-microphone method, *Journal of Sound and Vibration* 304 (2007) 91–109.
[11] G. Caignaert, J. Charley, Sources of uncertainties for hydroacoustic measurements in ducts, *Proceedings of the Symposium on Managing Uncertainties in Noise Measurements and Predictions*, Le Mans (France), 27–29 June 2005, CD paper 017, p. 8.
[12] M. Abom, H. Bodén, Error analysis of the two microphones measurements in ducts with flow, *Journal of the Acoustical Society of America* 83 (1988) 2429–2438.
[13] J.M. Jenkins, D.G. Watts, *Spectral Analysis*, Holden-Day, San Francisco, 1968.
[14] A.F. Seybert, Statistical errors in acoustic intensity measurements, *Journal of Sound and Vibration* 75 (1981) 519–526.
[15] J.-C. Pascal, FFT intensity meters used for sound sources and acoustical environment characterizations, *Inter-Noise 83 Proceedings*, Edinburgh (UK), 13–15 July 1983, pp. 1071–1074.
[16] F. Jacobsen, Random errors in sound intensity estimation, *Journal of Sound and Vibration* 128 (1989) 247–257.
[17] P.D. Welch, The use of Fast Fourier Transform for the estimation of power spectra: a method based on averaging over short modified periodograms, *IEEE Transactions on Audio and Electroacoustics* AU-15 (1967) 70–73.
[18] F.J. Harris, On the use of windows for harmonic analysis with the discrete Fourier transform, *Proceedings IEEE* 66 (1) (1978) 51–83.
[19] K. Macocco, Q. Grimal, S. Naïli, C. Soize, Probalistic modelling of an isotropic setup: calculation of the dispersion on wave speed measurements, *Comptes Rendus Mecanique* 333 (2005) 565–573 (in French with abridged English version).
[20] C.L. Morfey, Acoustic energy in non-uniform flows, *Journal of Sound and Vibration* 14 (1971) 159–169.